ENGINEERING

A durable nanomesh on-skin strain gauge for natural skin motion monitoring with minimum mechanical constraints

Yan Wang[1], Sunghoon Lee[1], Tomoyuki Yokota[1], Haoyang Wang[1], Zhi Jiang[1], Jiabin Wang[1], Mari Koizumi[1], Takao Someya[1,2]*

Ultraconformable strain gauge can be applied directly to human skin for continuous motion activity monitoring, which has seen widespread application in interactive robotics, human motion detection, personal health monitoring, and therapeutics. However, the development of an on-skin strain gauge that can detect human body motions over a long period of time without disturbing the natural skin movements remains a challenge. Here, we present an ultrathin and durable nanomesh strain gauge for continuous motion activity monitoring that minimizes mechanical constraints on natural skin motions. The device is made from reinforced polyurethane-polydimethylsiloxane (PU-PDMS) nanomeshes and exhibits excellent sustainability, linearity, and durability with low hysteresis. Its thinness geometry and softness provide minimum mechanical interference on natural skin deformations. During speech, the nanomesh-attached face exhibits skin strain mapping comparable to that of a face without nanomeshes. We demonstrate long-term facial stain mapping during speech and the capability for real-time stable full-range body movement detection.

INTRODUCTION

On-skin electronics are designed to be thin, soft, stretchable, and durable and can be seamlessly integrated to become part of the human body for continuous, long-term vital health monitoring (*1*–*5*). Among these electronics, strain gauges have attracted particular interest owing to their broad applications from human-machine interfaces to personal health diagnosis (*6*–*10*). In particular, soft, high-precision strain gauges have been applied for in vivo continuous measurements of organ function (*11*). Strain gauges have a simple mechanism, i.e., generating repetitive electrical changes upon mechanical deformations (*12*, *13*). They can be easily interfaced with soft biological systems for real-time health monitoring. The minimum requirements for these devices are high mechanical compliance, flexibility, sensitivity, stretchability, durability, light weight, thinness, and biocompatibility (*14*).

For practical implementation, strain gauges must conform to complex biological surfaces and sustain large deformations (>50% strain) during various activities. A plethora of intrinsically stretchable materials and engineered stretchable structures have been developed for this purpose (*15*, *16*). Typically, stretchable strain gauges are fabricated by depositing electrical metallic and/or carbon-based and/or liquid materials on a polymer substrate (*17*–*20*) or embedding them in a polymer matrix (*21*–*24*). For example, a representative bilayer structure made of aligned single-walled carbon nanotube/polydimethylsiloxane (PDMS) exhibits a stretchability of up to 280% strain, which is 50 times greater than that of traditional metal strain gauges (*25*). A composite structure composed of silver nanowire/PDMS can be stretched to 70% strain with a tunable gauge factor from 2 to 14 (*26*). Diverse innovative approaches of structural engineering have been introduced to soften gold and obtain stretchable nanomeshes for strain sensors (*27*). In addition to stretchability improvement, an ultrasensitive crack-based strain gauge has been fabricated from platinum and polyurethane acrylate with a gauge factor of over 2000 in 1 to 2% strain range (*28*). As ultrathinness is highly desirable for skin conformability, devices made of 2.56-μm-thick silicon nanomembrane/polyimide (PI) have been developed with a stretchability of 15% strain and a gauge factor of 0.5 (*29*). Moreover, a thinner epidermal strain gauge with a thickness of ~1 μm has been created from poly(3,4 ethylenedioxythiophene):poly(styrene sulfonate) (PEDOT:PSS) inkjet printed on a polystyrene-polybutadiene-polystyrene (SBS) nanosheet. The resulting device is capable of detecting 0 to 2% skin strain with a gauge factor of 0.73 ± 0.10 (*30*).

However, the development of an on-skin strain gauge that satisfies the requirement of negligible physical constraints on natural skin motions remains a challenge. First, it is difficult to obtain devices with porous/permeable substrates and a thickness of less than 2 μm that can also attain conformable contact with curvilinear human skin (*31*). The reason is that soft electronics made from porous/permeable substrates normally have thicknesses of more than 100 μm to achieve stretchability and mechanical durability (*32*–*34*). Second, the integration of functional metallic and/or carbon-based materials with traditional planar polymeric substrates leads to increased thickness. This is because a thin planar device can easily experience local material delamination/cracking under repetitive stretching/releasing cycles, especially under large strains. Furthermore, it is also necessary to increase device stretchability and sensitivity to allow for various degrees of human motion monitoring with high resolution.

Here, we report an ultrathin and durable nanomesh strain gauge for human movement detection while minimizing mechanical constraints on natural skin motions. The device is made from polyurethane (PU)–PDMS core-sheath–reinforced nanomeshes and has an ultralight weight of 0.12 mg/cm^2 with a thickness of only 430 ± 18 nm. It exhibits extraordinary mechanical durability of high-cycle stretching/releasing (5000 times) at up to 60% strain

[1]Department of Electrical Engineering and Information Systems, The University of Tokyo, 7-3-1 Hongo, Bunkyo-ku, Tokyo 113-8656, Japan. [2]Center for Emergent Matter Science (CEMS), RIKEN, 2-1 Hirosawa, Wako, Saitama 351-0198, Japan.
*Corresponding author. Email: someya@ee.t.u-tokyo.ac.jp

with a low-resistance degradation ($\Delta R/R_0$) of only 0.03. In addition, the reliable electrical responses are independent of the stretch frequencies with negligible hysteresis. Its thinness geometry and softness result in minimum mechanical constraints on natural skin motions. During speech, the nanomesh-attached face exhibits skin strain mapping comparable to that of a face without nanomeshes. We successfully demonstrated facial skin strain mapping in speech with minimum mechanical interference after long-term wearing (3.5 hours). Furthermore, a linear sensitivity of up to 60% strain enables stable full-range human body movement detection, including the subtle skin deformation by fingertip sensor pickup of the mechanical pulse wave at the human wrist and large joint bending motions.

RESULTS

Fabrication and characterization

The backbone of the permeable nanomesh sensor was fabricated by electrospinning PU nanofibers with a diameter of 198 ± 52 nm (fig. S1, A and B). In this study, an electrospinning volume of 0.5 ml was used, with a fraction area of 54.99 ± 2.16%. A schematic diagram of the fabrication process is shown in Fig. 1 (A to C) and described in Materials and Methods. Briefly, a PU nanofiber sheet was fixed with a PI window frame (125-μm thickness). Figure 1A shows the free-standing nanofiber sheet in the window region. Then, by dipping the PU nanofiber sheet into a diluted PDMS solution by hexane, the nanofibers formed random bundles and were encircled by the PDMS polymer after solvent evaporation (Fig. 1B). A mild ultraviolet (UV) ozone exposure (1 min) was subsequently used to render the surface hydrophilicity after the PDMS was fully cured. Last, the device was completed by gold deposition (100 nm) on both sides (Fig. 1C). It should be noted that the PI window is patternable, such that devices with arbitrary shapes can easily be achieved. The resulting device is ultralightweight (0.12 mg/cm^2), with a typical thickness of only 430 ± 18 nm, which substantially reduces the mass loading as an epidermal electronic (*35*). Figure 1 (D to F) shows representative microscopic views of the pristine PU nanofiber sheet, PU-PDMS core-sheath nanomesh, and Au/PU-PDMS nanomesh, respectively. Scanning electron microscopy (SEM) revealed an unambiguous PU-PDMS core-sheath mesh structure (fig. S1, C and D).

The PU nanofiber networks become interconnected owing to the PDMS coating, leading to enhanced structural integrity. As a consequence, the resultant mechanical strength of the freestanding PU-PDMS nanomesh is greatly improved, with larger stretchability compared with the bare PU nanofiber sheet (Fig. 1G). The tensile force for PU-PDMS nanomesh is 8.15 mN with a thickness of ca. 230 nm, at a tensile strain of 5%. This value is much smaller than that of the

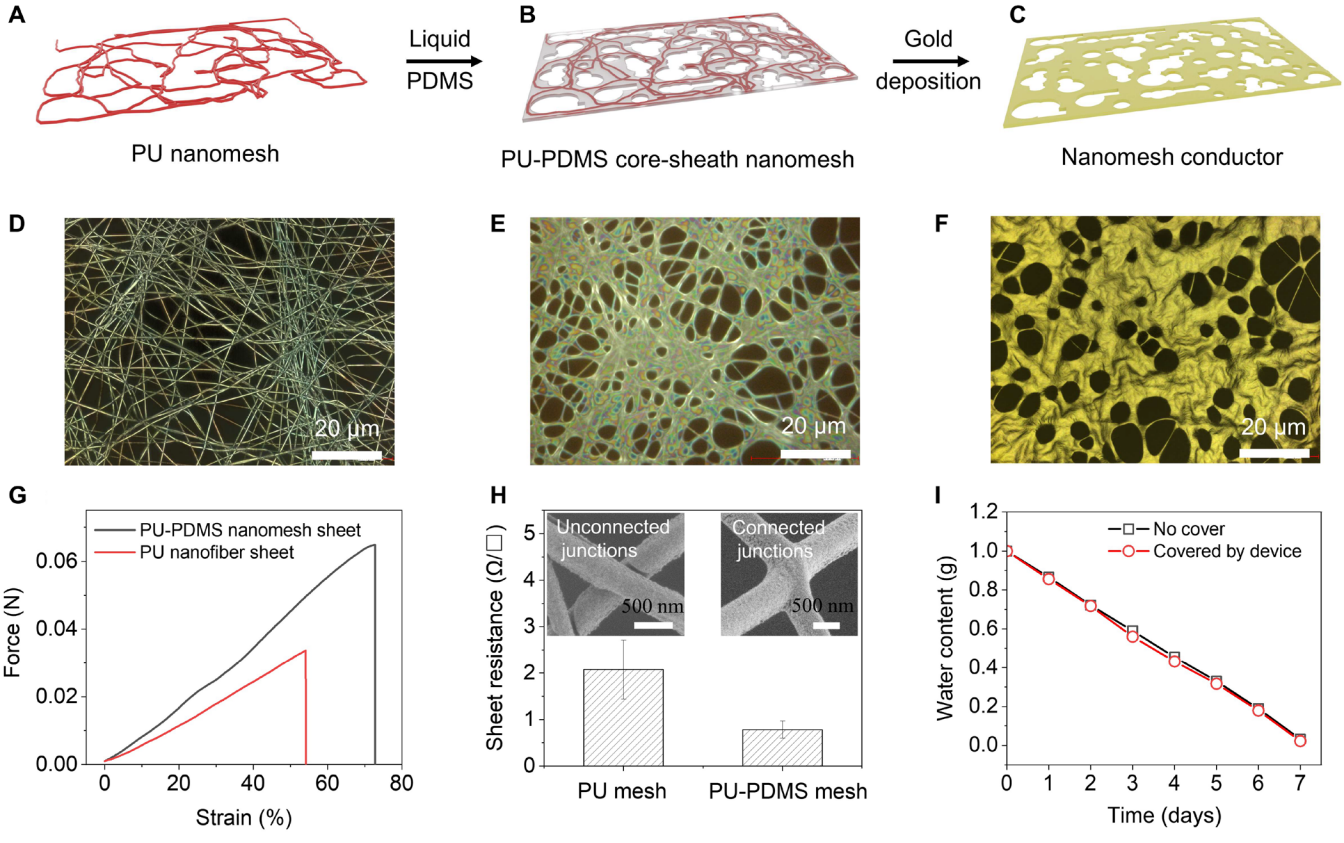

Fig. 1. Fabrication and characterization of PU-PDMS core-sheath nanomesh conductors. (**A** to **C**) Schematic of the fabrication process. (**D** to **F**) Corresponding microscopic images of the (D) PU nanofiber sheet, (E) PU-PDMS core-sheath nanomesh, and (F) Au/PU-PDMS nanomesh conductor. (**G**) Strain-stress curves of the bare PU nanofiber sheet and PU-PDMS nanomeshes. (**H**) Comparison of the sheet resistances of the bare PU nanomesh conductor and PU-PDMS nanomesh conductor ($N = 10$); the inset SEM images show the distinctive junction configurations of both devices. (**I**) Comparison of the water content of two bottles (one is not covered, and the other one is covered by the device).

continuous stratum corneum of human skin (*2*), which is 1.4 N with a thickness of 10 to 20 μm under the same strain level (*36*). In addition, the device has lower sheet resistance (1.2 ± 0.36 ohms/□) than the bare PU nanomesh conductor (2.03 ± 0.62 ohms/□) on account of the electrically connected junctions (see the inset SEM images in Fig. 1H). Further SEM illustrations are shown in fig. S1 (E to H).

To examine the gas permeability of the device, we performed a water vapor permeability test by measuring the weight loss as a function of time. An open glass bottle was used as a control, and another glass bottle was covered by the device. The water weight loss was measured, while the glass bottles were kept undisturbed in a thermostatic chamber (temperature, 25°C; relative humidity, 30%) for 1 week. The results show that the two bottles exhibit almost the same permeability (Fig. 1I).

Programmable stretchability and linear sensitivity

Different nanomesh structures could be effectively designed by changing the PDMS concentration in the diluted solution, thus obtaining nanomesh strain gauges with accustomed sensitivities and stretchabilities. In this study, PDMS/hexane ratios (w/w) of 1/40, 1/80, and 1/160 were applied, and microscopic images of the resultant nanomesh substrates are shown in fig. S2A. We will use the notations 1/40, 1/80, and 1/160 to indicate samples made from PDMS/hexane ratios (w/w) of 1/40, 1/80, and 1/160, respectively. Figure 2 (A to C) shows the corresponding devices after gold deposition. The surface profiles of the three conductors are depicted in Fig. 2D. The height plot shows a slight reduction from 0.56 ± 0.15 to 0.43 ± 0.18 μm because of the formation of thinner PU nanofiber bundles with more dilute PDMS solution (fig. S2B). Meanwhile, the area fracture of the mesh structure decreased gradually from 59.1 ± 2.23% to 31.3 ± 3.32% (Fig. 2E). However, all of the devices exhibited a similar pore size distribution with regard to its porous structure (Fig. 2F).

We then investigated the electromechanical performance of the device. It is known that different mesh structures will result in different stretchabilities and gauge factors (*37*). Gauge factor (GF), i.e., strain sensitivity, is defined as the ratio of the fractional change in electrical resistance to the fractional change in length. $\mathrm{GF} = \frac{\Delta R/R_0}{\Delta L/L_0} = \frac{\Delta R/R_0}{\varepsilon}$; here, ΔR and R are resistance change and original resistance, respectively. ΔL and L are length change and original length, respectively. ε is the applied strain. While being stretched uniaxially, the resistance of each device increased, but with different rates (fig. S2C).

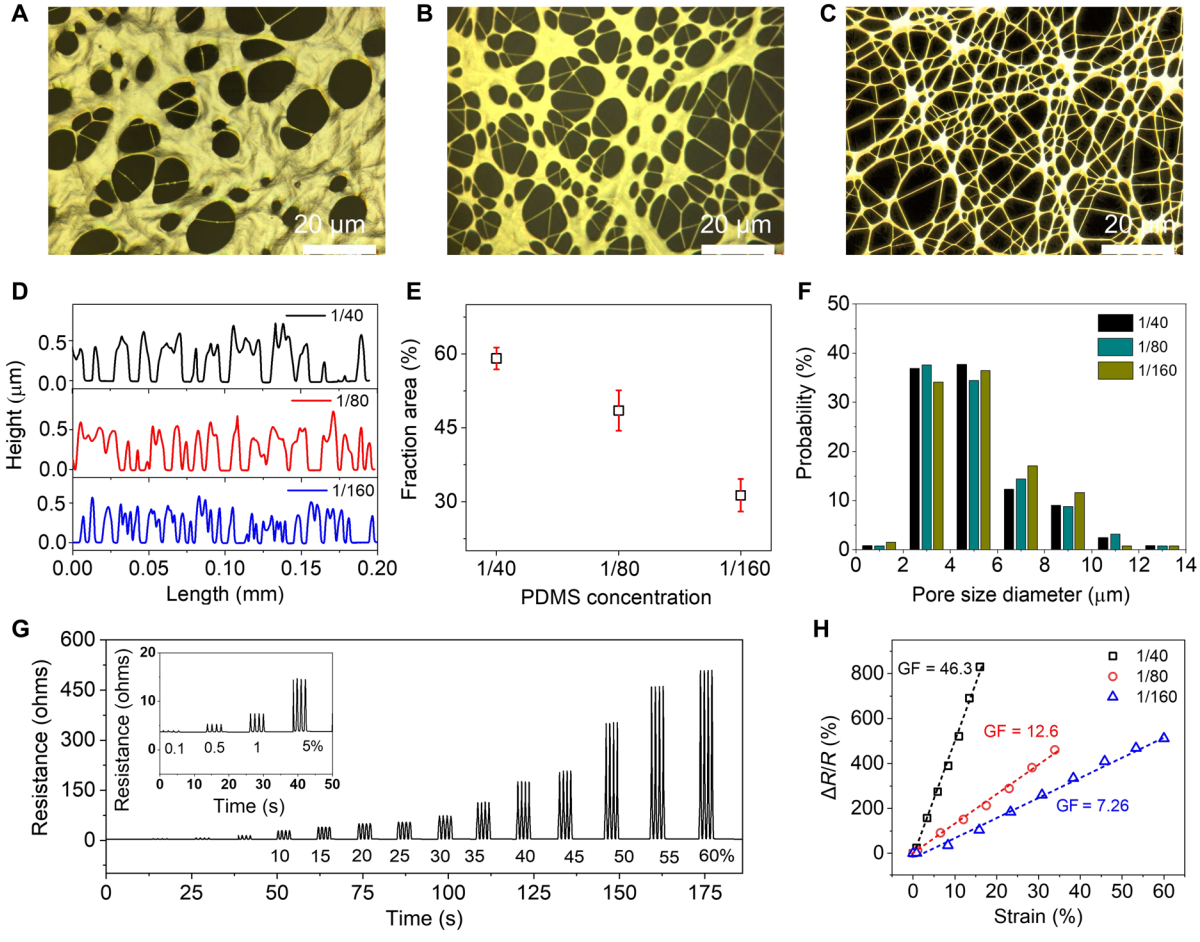

Fig. 2. Structural and electromechanical properties of three nanomesh strain gauges fabricated from different diluted PDMS solutions. (**A** to **C**) Microscopic characterization: (A) 1/40, (B) 1/80, and (C) 1/160 (w/w of PDMS/hexane). (**D**) Comparison of the surface profiles. (**E**) Comparison of the area fractions. (**F**) Comparison of the probability on pore size diameter. (**G**) Dynamic stretching/releasing electrical performance of the 1/40 sample in the strain range of 0.1 to 60%. (**H**) Linear sensitivities in the range of 0 to 16%, 0 to 35%, and 0 to 60% strain for the 1/40, 1/80, and 1/160 nanomesh sensors, respectively.

Device 1/160 experienced the lowest resistance increase under the same strain but had the largest stretchability of up to 150.2% strain. However, the 1/40 device had the largest resistance increase with the smallest stretchability of 77.9% strain as a result of the greatly reduced electrical junctions compared with the 1/160 nanomesh sensor. In conclusion, nanomesh strain gauges with different stretchabilities and sensitivities could be effectively programmed by changing the weight ratio of the diluted PDMS solution. The dynamic behavior of the sensor was examined in response to various strains from 0.1 to 60%, as shown in Fig. 2G.

Linearity is one of the key factors for stretchable strain gauges because it provides a simple and efficient calibration process compared with nonlinear stain sensors (*38*). It should be noted that linearity is normally limited to a certain range of strain for resistive-type strain gauges. Figure 2H demonstrates linear strain ranges of 16, 35, and 60% for the 1/40, 1/80, and 1/160 devices, respectively, which is sufficiently large to realize the detection of different degrees of human body movements. Furthermore, the gauge factors range from 46.3 to 7.26, which are sufficient to achieve high-resolution motion detection of various human movements.

Figure S3 (A to F) shows changes in the surface morphology of the 1/160 nanomesh sensor while stretching incrementally from 0 to 150% strain and releasing back to its original state. At low strains, the nanomesh started to elongate parallel to the applied strain (horizontally), and nanocracks began to appear on the nanomeshes. At this point, linear resistance changes were observed (Fig. 2H), and the structural changes were mainly attributed to the elongation of the nanomeshes. Further increasing the strain escalated the overall stretching of the device, and the straightened PU-PDMS core-sheath fibers started to show small reversible fractures, with the formation of visible cracks on the gold layer perpendicular to the strain direction. This led to substantial resistance changes in the nanomesh sensors under large strain. The structural integrity is maintained well at large strains (see the SEM characterization in fig. S3G). At even higher strains beyond the tolerable range, disconnections between the PU-PDMS meshes became noticeable, leading to nanomesh breakage (fig. S3H). The nanomesh structure was retained upon strain releasing (fig. S3F).

Electromechanical sustainability, reliability, and durability

To investigate the hysteresis behavior of the nanomesh strain gauges, we subjected a dynamic strain (16%) at a frequency of 1 Hz to the nanomesh sensor and recorded the electrical response at the same time. The degree of hysteresis was calculated to be 6.1% (fig. S2D) (*39*).

For the sustainability evaluation, we applied the device with a strain of 40% and held for a duration of 12 hours (Fig. 3, A to C). In response to the long-term constant static stretching, the resistance of the nanomesh sensor drifted from R_1 (19.61 ohms) to R_2 (18.56 ohms), with an electrical drift error (defined as $\frac{R_1 - R_2}{R_1}$) of less than 0.053, i.e., 5.3%. In addition, the resistance returned to its original value of 6.16 ohms after strain releasing. Figure 3 (A to C) also shows no overshooting behavior of the device, which is a common issue for resistive strain gauges (*25*). Moreover, this good uniform electrical response is independent of the stretching frequencies from 0.5 to 3.1 Hz (Fig. 3D). Cyclic tests were performed to further demonstrate the mechanical durability of our device. Figure 3E describes cyclic stretching/releasing to 60% strain for 5000 cycles. Specifically, the resistance degradation value is low to 0.03, which is 30,000 times lower than that of a previously reported film-type on-skin strain

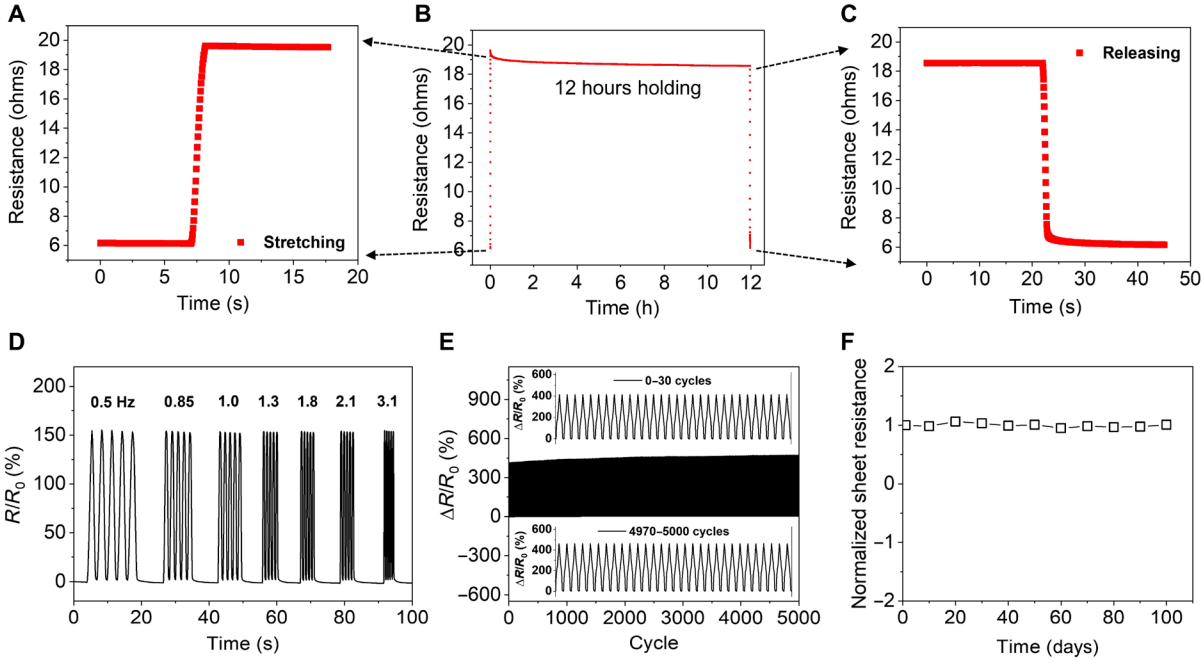

Fig. 3. Device sustainability, durability, and long-term stability. (**A** to **C**) Reliable and reversible electrical responses for 12 hours of continuous stretching under 40% strain. (**D**) Uniform and repeatable electrical responses under 30% strain at frequencies from 0.6 to 3.1 Hz. (**E**) Cyclic stretching/releasing for 5000 cycles at 60% strain; the insets show 0 to 30 and 4970 to 5000 cycles, respectively (frequency = 1 Hz). (**F**) Stable conductivity over more than 3 months of storage under ambient conditions (w/w ratio of PDMS/hexane: 1/160).

gauge made from carbon nanotube/PDMS (50% strain, 100 cycles) (*40*) and three times lower than that of a nanomesh strain gauge made from Ag nanowires (AgNWs)/PU (70% strain, 1000 cycles) (*41*). There is slight hysteresis in resistance in the first few hundreds of cycles owing to the mechanical properties of PDMS, with R_{max} increased by 0.083 times after 5000 stretching/releasing cycles under 60% strain (*13*). Furthermore, the sheet resistance of the PU-PDMS nanomesh was stable over 100 days of storage under ambient conditions owing to the inertness of gold, demonstrating a long-term shelf life as in potential practical usage (Fig. 3F).

Durability tests were also conducted on three other nanomesh sensors fabricated from different nanofiber scaffolds: polyvinyl alcohol (PVA), PU, and PU with Parylene coating (see SEM images in fig. S4, A to C). The sample preparation and sizes were kept the same (see Materials and Methods). Unlike the other three nanomeshes, the reinforced PU-PDMS nanomeshes exhibited uniform cyclic straining for 100 cycles at the same strain level of 30% (fig. S4, D to H). In particular, the substrate-free PVA nanomesh system showed limited stretchability. The bare PU nanomesh structures were severely damaged, and enormous permanent cracks occurred and increased, leading to notable influence on the electrical responses under repetitive stretching/releasing (fig. S4I).

On-skin strain gauge

We used a spin-coated biocompatible PVA film or PVA nanofiber sheet (*42*) as a sacrificial support for easy manipulation. After the nanomesh device is attached to human skin and sprayed with water mist, the PVA layer will be readily dissolved, and the device will adhere to the skin. Figure S5 shows microscopic images of the device on a fingertip replica, demonstrating distinct sweat pore features of human skin. Such intimate contact is barely perceptible to the subject when wearing the device.

Facial tissues are one of the softest parts of human skin, which involves numerous micromovements and moderate deformations (~20% strain) across the face during speech (*43*). Face sensor–based speech recognition system enables private, nondisturbing communication regardless of environmental noise. We evaluated the strain mapping of facial skin deformations during speech using nanomesh sensors and compared the results with film-type PDMS samples. The experimental details are described in Materials and Methods and fig. S6. Briefly, nanomesh sensors are attached on the right side of the face, while black rectangle markers are placed on the left side of the face as a reference. The deformations of the black markers represent the natural deformations of skin. The strain mappings are attributed to the nonhomogeneous face strain distribution under each phonation. When both sides of the face were marked with black markers, the strain mapping results (fig. S7, A to I) evidence the symmetrical, topographical skin movements on the two sides of the face during the speech of "a," "u," and "o." Then, the nanomesh sensor strains on the right side of the face was measured during different phonations in the same manner to compare with that of the black markers on the left side of the face (fig. S8). The result also looks symmetrical, which indicates that the deformations of nanomesh sensors reflect face skin deformations, the same as the black markers. On the other hand, the right side of the face with attached film-type PDMS samples shows serious strain impediments compared with that of the left side of the face with the black markers (fig. S7, J to R). Specifically, during phonations of "a," "u," and "o," the highest strains for black markers were 17.5 to 18.8%, 22.5 to 25.0%, and 22.5 to 25.0%, respectively, and 18.3, 23.6, and 21.7% for nanomesh strain gauges, respectively. However, in terms of PDMS films, the corresponding values decreased seriously to 1.3, 3.8, and 2.5%, respectively. Further, we compared the strain mapping results derived from the sensing results from the nanomesh sensors on the right side of the face to that of the left side of the face with black markers (Fig. 4). Figure 4 shows that the skin strain distribution on the right side of the face also looks symmetrical to the left side of the face with the black markers. The results indicate that our nanomesh devices reflect the actual skin deformations with minimal mechanical constraints, the skin with nanomeshes can still be strained and compressed freely during speech (fig. S9A). This excellent conformability originates from the thinness geometry, ultralight weight, and softness of the devices, which leads to imperceptible contact with curvilinear skin. In contrast, film-type samples either suppressed the skin strain or experienced slippage because of poor mechanical compliance (fig. S9B). The conformable nanomesh strain gauges proved to be functional even after being worn on the subject's face for 3.5 hours during normal daily life (fig. S10). The subject did not report any discomfort or negative sensations at the attachment sites while engaging daily life activities (*42*).

We then used highly sensitive 1/40 PU-PDMS nanomeshes to detect the subtle skin deformation on the human wrist induced by pulse. Figure S11A shows that the device flows naturally along the curvilinear free edges on the fingertip. By gently pressing the radial artery with the attached device, the amplitude and frequency of the resistance changes could be readily picked up in real time (fig. S11B). Signals obtained before and after physical exercise comprising a 1-min squat show distinct wave features, with heartbeats of 54 and 60 beats/min, respectively. Two distinct peaks (P_1 and P_3) and a late systolic augmentation shoulder (P_2) were observed in the wrist pulse wave before physical exercise (*44*), while there was no P_2 peak in the signals obtained after physical exercise (fig. S11, C and D). The radial augmentation index (AIr = P_2/P_1) signifies arterial stiffness, which is highly influenced by the age of the individual (*44*). The average AIr value derived from our results is 0.68, which is in good agreement with the literature for a 30-year-old healthy female.

In addition to subtle skin deformation, the device with higher linear stretchability (1/160) is also capable of detecting large joint bending motions. The device was laminated on the joint at the back of the human wrist. High stretchability and excellent compliance of the system are crucial for avoiding breakage or detachment from the skin when the wrist is bent to a large degree (fig. S11E). The actual skin strains were measured to be 11.1, 22.2, and 33.3% for 30°, 60°, and 90° wrist bending, respectively, matching well with the calculated strain of 11.2, 22.1, and 33.6% based on relative resistance change. We further investigated the mechanical durability by cyclic wrist flexion. The strain sensor maintained the functionality even after 10,000 bending/relaxing cycles (fig. S12, A and B). Figure S12C shows microscopic characterizations of the device under three states of the participant's wrist (flat, 90° bending, flat) after 10,000-cycle fatigue tests, demonstrating the well-maintained structural integrity of the nanomesh and device conformability with the skin after long-term cyclic testing.

DISCUSSION

Compared to our previous work (*45*), in which ultrasoft multilayered nanomeshes comprising PU, Parylene, and Au were developed to

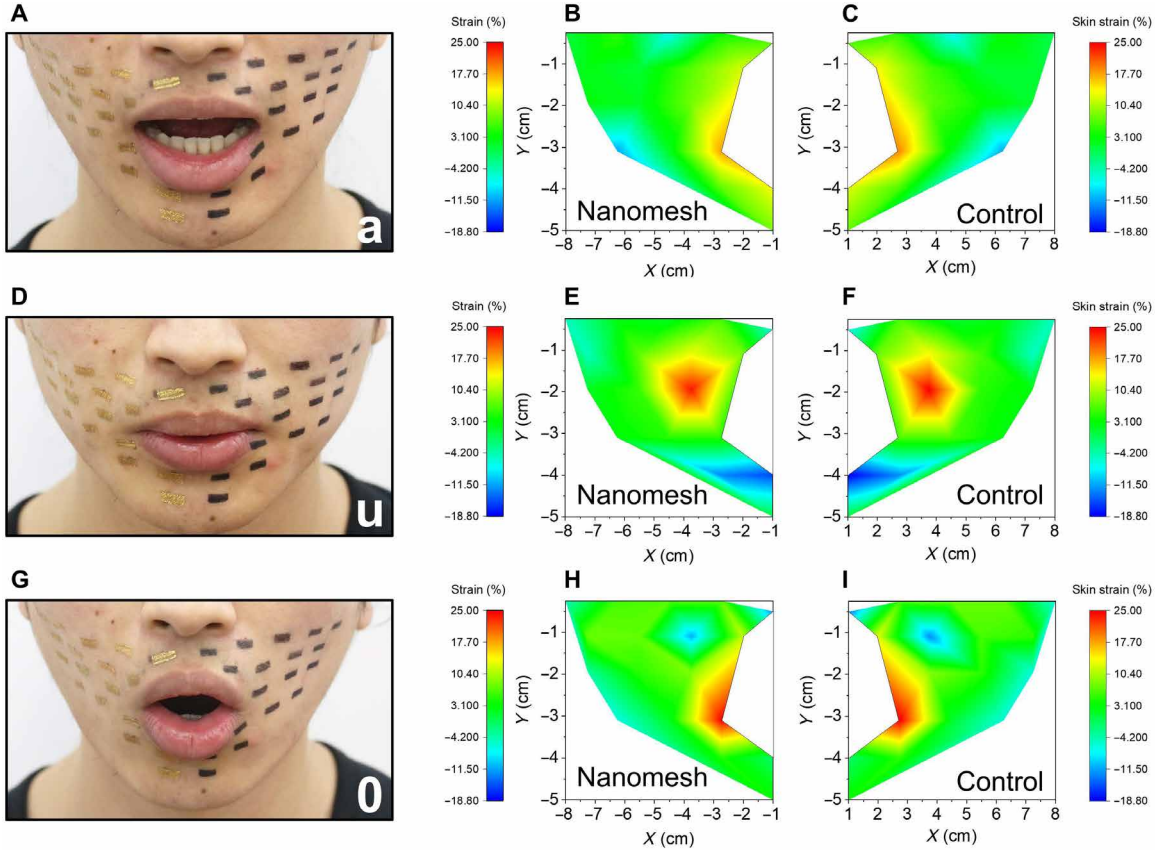

Fig. 4. Facial skin strain mapping during speech of "a," "u," and "o" with nanomesh sensors on the right side of the face and black markers on the left side of the face. (**A**) Photograph of a face during speech of "a." (**B**) Strain mapping of the right side of the face during speech of "a." (**C**) Strain mapping of the left side of the face during speech of "a." (**D**) Photograph of a face during speech of "u." (**E**) Strain mapping of the right side of the face during speech of "u." (**F**) Strain mapping of the left side of the face during speech of "u." (**G**) Photograph of a face during speech of "o." (**H**) Strain mapping of the right side of the face during speech of "o." (**I**) Strain mapping of the left side of the face during speech of "o." Photo credit (A, D, and G): Yan Wang; The University of Tokyo.

quantitatively characterize dynamically pulsing cardiomyocytes, the present PU-PDMS nanomeshes are designed to be thinner and more stretchable for use as an on-skin strain gauge that can move freely and spontaneously with human curvilinear skin during full-range human body movements. The remarkable durability results from the sustainability and cyclic stretching and flexure tests are successfully demonstrated. Mechanical durability is strongly desired with regard to long-term, high-precision, and reliable real skin motion monitoring, which is of high significance for other practical applications such as remote personal health monitoring, endurance sports performance tracking, and prosthetics. Considering the fabrication efficiency and economical issue for practical technology translation, it is promising to replace thermal evaporation of Au layer with direct coating of conductive nanomaterials or in situ polymerization of electrospun nanofibers (*46*) to construct nanomesh electronics in the future. A detailed performance comparison with representative recently reported skin-mountable sensors is presented in table S1 (*13*, *40*–*42*, *47*–*51*). Nanomesh sensor from this work is advantageous in features such as weight, linear strain range, and durability in addition to gas permeability and thinness. We envisage that our imperceptible and high-performance nanomesh sensors may become an important component in future skin-on/implantable electronics for everyday, continuous, long-term, stable health monitoring.

MATERIALS AND METHODS

PDMS/hexane diluted solution

The SYLGARD 184 silicone elastomer base and the curing agent were mixed at a weight ratio of 10:1. Ratios of PDMS diluted in hexane (w/w) of 1/40, 1/80, and 1/160 were used. Thin PDMS films were obtained by spin coating a pure PDMS precursor and cured at 60°C for 2 hours in an oven.

Fabrication of the nanomesh sensors

The fabrication process for the PU nanofibers was modified from a previous report (*45*). A pristine PU solution (Rezamin M-8115LP) was from Dainichiseika, Japan [30 weight % (wt %)]. A 13 wt % PU solution was prepared by dilution with a mixed solvent (*N*,*N*-dimethylformamide:methyl ethyl ketone at a ratio of 7:3) and subsequently stirred for 2 hours at room temperature (22° to 25°C) in a dark environment. The as-prepared PU solution was placed in a glass syringe with a 27-gauge-diameter metallic needle. The PU nanofiber sheet was prepared by electrospinning (Fuence ES-2000, Japan) at a voltage of 25 kV. The distance between the needle tip and grounded collector was 12.5 cm. The solution was injected at a flow rate of 0.1 ml/hour and collected on a silicone-coated paper for easy delamination. A freestanding PU nanofiber sheet could be obtained by transferring the PU nanofiber sheet onto the PI

substrate with a window frame of 15 × 25 mm^2. Then, the PU nanomesh was dipped into a diluted PDMS solution and fully cured at 60°C for 5 min in an oven to obtain the PU-PDMS core-sheath nanomesh. Next, a mild UV ozone exposure (1 min) was used to render the surface hydrophilicity. Last, the device was completed by depositing a 100-nm-thick Au layer on both sides using a thermal evaporator.

Optical microscope and digital images were recorded using a Nikon Eclipse LV150 microscope and Nikon camera, respectively. On-skin microscopic images were obtained using a mobile digital microscope from Dino-Lite, Japan. SEM imaging was carried out using a FEI Helios Nanolab 600 FIB (focused ion beam)–SEM operating at a voltage of 1 kV. The fingertip replicas were made using a two-part mixed-type replica agent (Silflo, Amic Group, Japan). The sheet resistance measurements were carried out on a Jandel four-point conductivity probe using a linearly arrayed four-point head. Pore size distribution result is derived from optical microscopic images of the device surface using an image analyzer (ImageJ).

Fabrication of the sensor patch for facial strain mapping

The sensor patch consisted of a sensing part (relative high resistance, strain sensitive) and contact pads (low resistance, strain insensitive) (fig. S6). We chose 1/160 PU-PDMS because of its higher linear strain range. Au thickness was 70 nm. The contact pad (~1.5 × 3 mm^2) was constructed by the introduction of AgNWs (*41*) (dip coating) at the two ends of Au/PU-PDMS nanomeshes (fig. S6). AgNWs were from ACS Material, Japan, with a diameter of 30 nm and a length of 100 to 200 μm.

Tensile stress tests

For mechanical characterization of the freestanding PU and PU-PDMS nanomesh sheets, samples were prepared in a similar manner to that for the fabrication of nanomesh conductors without metal deposition. The nanomesh sheet was transferred to a PI film with a window with dimensions of 5 mm in height and 10 mm in width. Next, the samples were fixed to the top and bottom clamps of a tensile tester (AG-X, Shimadzu, Japan), the nanomesh and PI on the left and right borders were separated with a sharp tweezer and carefully cut off the PI on the two sides (transversely). Then, the tensile stress was examined at a speed of 10 mm/min.

Evaluation of water vapor permeability

The water vapor permeability was evaluated by measuring the weight of water in glass bottle covered by the device. PDMS in hexane (1/40 w/w) was used in this experiment because it had the lowest porosity. Milli-Q water (1 g) was stored in a glass bottle with a diameter of 15 mm at the opening. The nanomesh conductor sheet was used to cover the opening of the bottle. The bottle was left undisturbed in a thermostatic chamber at 25°C and a humidity of 30% for 1 week, and the water weight loss was measured. A bottle without any covering was used as the reference sample.

Stretchability test

A PDMS film with a thickness of 200 μm was used as the substrate. Laminate the nanomeshes to the PDMS substrate after adding an adhesive layer in between by spin coating PDMS/hexane solution (w/w: 1/10) at 2000 rpm for 30 s. Then, the device was cured at 60°C for 5 min in an oven. It is noted that there is negligible change in the sheet resistance after lamination onto the PDMS substrate. Next, the two ends of the samples were attached to motorized moving stages (Thorlabs model LTS150/M, USA). Uniform stretching/releasing cycles were then applied by a computer-based user interface (Thorlabs APT user), while the resistance changes were recorded using a digital multimeter (34410A Agilent, USA). Note that the sample size is kept the same: a width of 3 mm and a length of 5 mm.

PVA nanomesh conductor

The fabrication process for the PVA nanomesh conductors was modified from a previous report (*42*). Here, a 1.5-ml volume of solution was used for electrospinning. The Au thickness was 100 nm.

PU nanomesh with Parylene-coated conductor

A 0.5-ml volume of PU solution was used for electrospinning. Then, a 200-nm-thick Parylene layer was coated onto the PU nanofiber sheet through chemical vapor deposition. The Au thickness was 100 nm.

Facial skin strain mapping

Three kinds of samples (nanomesh sensor, 200-μm-thick PDMS film, and black marker) were placed on the face in a symmetrical way. On each side of the face, there were 18 nanomesh sensors or PDMS films or black markers. The placement of each sample was controlled by a patterned PI mask. The sample size was ~3 × 8 mm^2. Vertical and the horizontal distances were 18 and 10 mm, respectively. The subject remained immobile in each state during measurement. The sample lengths were measured one by one for the 18 positions with a ruler before and after phonations of "a," "u," and "o" (figs. S7 and S8 and results of black markers in fig. S10 and Fig. 4). The strain result was calculated to be the ratio of length change by the initial length value in silence. The resistance of 18 nanomesh strain sensors was recorded one by one by a multimeter directly contacting with contact pads (results of nanomesh strain sensors in Fig. 4 and fig. S10). The calculated strain values were derived by the resistance and gauge factor from the strain sensors. The heatmap was analyzed and performed via contour mapping using Origin software by gathering strain results from all samples on one side of the face. The subject engaged normal daily life activities during the 3.5-hour wearing in the durability test. The strain results were averages of three measurements.

Breathable on-skin strain gauge (wrist pulse and flexure monitoring)

Flexible anisotropic conductive films were used to connect the strain gauge and conductive wires; the conductive wires were then connected to a digital multimeter (34410A, Agilent) for resistance measurements. In wrist pulse monitoring, the nanomesh sensor was attached on the index fingertip of the right hand, and then the resistance signals were collected while pressing the wrist pulse on the left hand with the attached sensor. In the 10,000-cycle wrist bending/relaxing experiment, the interval between each bending was ~1 s; the applied bending degree was random.

All experiments for this project were thoroughly reviewed and approved by the ethical committee of The University of Tokyo (approval numbers KE19-33 and KE19-32).

SUPPLEMENTARY MATERIALS

Supplementary material for this article is available at http://advances.sciencemag.org/cgi/content/full/6/33/eabb7043/DC1

REFERENCES AND NOTES

1. J. A. Rogers, T. Someya, Y. Huang, Materials and mechanics for stretchable electronics. *Science* **327**, 1603–1607 (2010).
2. T. Someya, M. Amagai, Toward a new generation of smart skins. *Nat. Biotechnol.* **37**, 382–388 (2019).
3. X. Wang, L. Dong, H. Zhang, R. Yu, C. Pan, Z. L. Wang, Recent progress in electronic skin. *Adv. Sci.* **2**, 1500169 (2015).
4. M. Kondo, M. Melzer, D. Karnaushenko, T. Uemura, S. Yoshimoto, M. Akiyama, Y. Noda, T. Araki, O. Schmidt, T. Sekitani, Imperceptible magnetic sensor matrix system integrated with organic driver and amplifier circuits. *Sci. Adv.* **6**, eaay6094 (2020).
5. W. Gao, S. Emaminejad, H. Y. Y. Nyein, S. Challa, K. Chen, A. Peck, H. M. Fahad, H. Ota, H. Shiraki, D. Kiriya, Fully integrated wearable sensor arrays for multiplexed in situ perspiration analysis. *Nature* **529**, 509–514 (2016).
6. C. Pang, G. Y. Lee, T. I. Kim, S. M. Kim, H. N. Kim, S. H. Ahn, K. Y. Suh, A flexible and highly sensitive strain-gauge sensor using reversible interlocking of nanofibres. *Nat. Mater.* **11**, 795–801 (2012).
7. Y. Wu, I. Karakurt, L. Beker, Y. Kubota, R. Xu, K. Y. Ho, S. Zhao, J. Zhong, M. Zhang, X. Wang, Piezoresistive stretchable strain sensors with human machine interface demonstrations. *Sens. Actuator A Phys.* **279**, 46–52 (2018).
8. T. Yang, X. Li, X. Jiang, S. Lin, J. Lao, J. Shi, Z. Zhen, Z. Li, H. Zhu, Structural engineering of gold thin films with channel cracks for ultrasensitive strain sensing. *Mater. Horiz.* **3**, 248–255 (2016).
9. H. J. Kim, K. Sim, A. Thukral, C. Yu, Rubbery electronics and sensors from intrinsically stretchable elastomeric composites of semiconductors and conductors. *Sci. Adv.* **3**, e1701114 (2017).
10. X. Li, T. Yang, Y. Yang, J. Zhu, L. Li, F. E. Alam, X. Li, K. Wang, H. Cheng, C. T. Lin, Large-area ultrathin graphene films by single-step marangoni self-assembly for highly sensitive strain sensing application. *Adv. Funct. Mater.* **26**, 1322–1329 (2016).
11. A. D. Mickle, S. M. Won, K. N. Noh, J. Yoon, K. W. Meacham, Y. Xue, L. A. McIlvried, B. A. Copits, V. K. Samineni, K. E. Crawford, A wireless closed-loop system for optogenetic peripheral neuromodulation. *Nature* **565**, 361–365 (2019).
12. J. Park, Y. Lee, J. Hong, M. Ha, Y. D. Jung, H. Lim, S. Y. Kim, H. Ko, Giant tunneling piezoresistance of composite elastomers with interlocked microdome arrays for ultrasensitive and multimodal electronic skins. *ACS Nano* **8**, 4689–4697 (2014).
13. Y. R. Jeong, H. Park, S. W. Jin, S. Y. Hong, S. S. Lee, J. S. Ha, Highly stretchable and sensitive strain sensors using fragmentized graphene foam. *Adv. Funct. Mater.* **25**, 4228–4236 (2015).
14. C. Yan, J. Wang, W. Kang, M. Cui, X. Wang, C. Y. Foo, K. J. Chee, P. S. Lee, Highly stretchable piezoresistive graphene–nanocellulose nanopaper for strain sensors. *Adv. Mater.* **26**, 2022–2027 (2014).
15. J. Park, I. You, S. Shin, U. Jeong, Material approaches to stretchable strain sensors. *ChemPhysChem* **16**, 1155–1163 (2015).
16. N. N. Jason, M. D. Ho, W. Cheng, Resistive electronic skin. *J. Mater. Chem C.* **5**, 5845–5866 (2017).
17. E. Roh, B. U. Hwang, D. Kim, B. Y. Kim, N. E. Lee, Stretchable, transparent, ultrasensitive, and patchable strain sensor for human–machine interfaces comprising a nanohybrid of carbon nanotubes and conductive elastomers. *ACS Nano* **9**, 6252–6261 (2015).
18. X. Liao, Q. Liao, X. Yan, Q. Liang, H. Si, M. Li, H. Wu, S. Cao, Y. Zhang, Flexible and highly sensitive strain sensors fabricated by pencil drawn for wearable monitor. *Adv. Funct. Mater.* **25**, 2395–2401 (2015).
19. D. J. Lipomi, M. Vosgueritchian, B. C. Tee, S. L. Hellstrom, J. A. Lee, C. H. Fox, Z. Bao, Skin-like pressure and strain sensors based on transparent elastic films of carbon nanotubes. *Nat. Nanotechnol.* **6**, 788–792 (2011).
20. Z. Liu, D. Qi, P. Guo, Y. Liu, B. Zhu, H. Yang, Y. Liu, B. Li, C. Zhang, J. Yu, L. Bo, X. Chen, Thickness-gradient films for high gauge factor stretchable strain sensors. *Adv. Mater.* **27**, 6230–6237 (2015).
21. Y. Wang, S. Gong, S. J. Wang, G. P. Simon, W. Cheng, Volume-invariant ionic liquid microbands as highly durable wearable biomedical sensors. *Mater. Horiz.* **3**, 208–213 (2016).
22. M. Zhang, C. Wang, H. Wang, M. Jian, X. Hao, Y. Zhang, Carbonized cotton fabric for high-performance wearable strain sensors. *Adv. Funct. Mater.* **27**, 1604795 (2017).
23. J. T. Muth, D. M. Vogt, R. L. Truby, Y. Mengüç, D. B. Kolesky, R. J. Wood, J. A. Lewis, Embedded 3D printing of strain sensors within highly stretchable elastomers. *Adv. Mater.* **26**, 6307–6312 (2014).
24. F. Xu, Y. Zhu, Highly conductive and stretchable silver nanowire conductors. *Adv. Mater.* **24**, 5117–5122 (2012).
25. T. Yamada, Y. Hayamizu, Y. Yamamoto, Y. Yomogida, A. Izadi Najafabadi, D. N. Futaba, K. Hata, A stretchable carbon nanotube strain sensor for human-motion detection. *Nat. Nanotechnol.* **6**, 296–301 (2011).
26. M. Amjadi, A. Pichitpajongkit, S. Lee, S. Ryu, I. Park, Highly stretchable and sensitive strain sensor based on silver nanowire–elastomer nanocomposite. *ACS Nano* **8**, 5154–5163 (2014).
27. B. Zhu, S. Gong, W. Cheng, Softening gold for elastronics. *Chem. Soc. Rev.* **48**, 1668–1711 (2019).
28. D. Kang, P. V. Pikhitsa, Y. W. Choi, C. Lee, S. S. Shin, L. Piao, B. Park, K. Y. Suh, T. I. Kim, M. Choi, Ultrasensitive mechanical crack-based sensor inspired by the spider sensory system. *Nature* **516**, 222–226 (2014).
29. D. Son, J. Lee, S. Qiao, R. Ghaffari, J. Kim, J. E. Lee, C. Song, S. J. Kim, D. J. Lee, S. W. Jun, Multifunctional wearable devices for diagnosis and therapy of movement disorders. *Nat. Nanotechnol.* **9**, 397–404 (2014).
30. Y. Tetsu, K. Yamagishi, A. Kato, Y. Matsumoto, M. Tsukune, Y. Kobayashi, M. G. Fujie, S. Takeoka, T. Fujie, Ultrathin epidermal strain sensor based on an elastomer nanosheet with an inkjet-printed conductive polymer. *Appl. Phys. Express.* **10**, 087201 (2017).
31. M. Kaltenbrunner, T. Sekitani, J. Reeder, T. Yokota, K. Kuribara, T. Tokuhara, M. Drack, R. Schwödiauer, I. Graz, S. Bauer Gogonea, An ultra-lightweight design for imperceptible plastic electronics. *Nature* **499**, 458–463 (2013).
32. G. S. Jeong, D. H. Baek, H. C. Jung, J. H. Song, J. H. Moon, S. W. Hong, I. Y. Kim, S. H. Lee, Solderable and electroplatable flexible electronic circuit on a porous stretchable elastomer. *Nat. Commun.* **3**, 1–8 (2012).
33. B. Sun, R. N. McCay, S. Goswami, Y. Xu, C. Zhang, Y. Ling, J. Lin, Z. Yan, Gas-permeable, multifunctional on-skin electronics based on laser-induced porous graphene and sugar-templated elastomer sponges. *Adv. Mater.* **30**, 1804327 (2018).
34. Y. Xu, B. Sun, Y. Ling, Q. Fei, Z. Chen, X. Li, P. Guo, N. Jeon, S. Goswami, Y. Liao, Multiscale porous elastomer substrates for multifunctional on-skin electronics with passive-cooling capabilities. *Proc. Natl. Acad. Sci. U.S.A.* **117**, 205–213 (2020).
35. D. H. Kim, N. Lu, R. Ma, Y. S. Kim, R. H. Kim, S. Wang, J. Wu, S. M. Won, H. Tao, A. Islam, Epidermal electronics. *Science* **333**, 838–843 (2011).
36. K. Koutroupi, J. Barbenel, Mechanical and failure behaviour of the stratum corneum. *J. Biomech.* **23**, 281–287 (1990).
37. Y. Wang, S. Gong, D. Dong, Y. Zhao, L. W. Yap, Q. Shi, T. An, Y. Ling, G. P. Simon, W. Cheng, Self-assembled gold nanorime mesh conductors for invisible stretchable supercapacitors. *Nanoscale* **10**, 15948–15955 (2018).
38. M. Amjadi, K. U. Kyung, I. Park, M. Sitti, Stretchable, skin-mountable, and wearable strain sensors and their potential applications: A review. *Adv. Funct. Mater.* **26**, 1678–1698 (2016).
39. D. Y. Choi, M. H. Kim, Y. S. Oh, S. H. Jung, J. H. Jung, H. J. Sung, H. W. Lee, H. M. Lee, Highly stretchable, hysteresis-free ionic liquid-based strain sensor for precise human motion monitoring. *ACS Appl. Mater. Interfaces* **9**, 1770–1780 (2017).
40. N. Lu, C. Lu, S. Yang, J. Rogers, Highly sensitive skin-mountable strain gauges based entirely on elastomers. *Adv. Funct. Mater.* **22**, 4044–4050 (2012).
41. Z. Jiang, M. O. G. Nayeem, K. Fukuda, S. Ding, H. Jin, T. Yokota, D. Inoue, D. Hashizume, T. Someya, Highly stretchable metallic nanowire networks reinforced by the underlying randomly distributed elastic polymer nanofibers via interfacial adhesion Improvement. *Adv. Mater.* **26**, 1903446 (2019).
42. A. Miyamoto, S. Lee, N. F. Cooray, S. Lee, M. Mori, N. Matsuhisa, H. Jin, L. Yoda, T. Yokota, A. Itoh, M. Sekino, H. Kawasaki, T. Ebihara, M. Amagai, T. Someya, Inflammation-free, gas-permeable, lightweight, stretchable on-skin electronics with nanomeshes. *Nat. Nanotechnol.* **12**, 907–913 (2017).
43. V. Luboz, E. Promayon, Y. Payan, Linear elastic properties of the facial soft tissues using an aspiration device: Towards patient specific characterization. *Ann. Biomed. Eng.* **42**, 2369–2378 (2014).
44. W. W. Nichols, Clinical measurement of arterial stiffness obtained from noninvasive pressure waveforms. *Am. J. Hypertens.* **18**, 3S–10S (2005).
45. S. Lee, D. Sasaki, D. Kim, M. Mori, T. Yokota, H. Lee, S. Park, K. Fukuda, M. Sekino, K. Matsuura, Ultrasoft electronics to monitor dynamically pulsing cardiomyocytes. *Nat. Nanotechnol.* **14**, 156–160 (2019).
46. X. Li, W. Liu, S. Liu, M. Li, Y. Li, M. Ge, In situ polymerization of aniline in electrospun microfibers. *Chin. Chem. Lett.* **25**, 83–86 (2014).
47. S. Choi, S. I. Han, D. Jung, H. J. Hwang, C. Lim, S. Bae, O. K. Park, C. M. Tschabrunn, M. Lee, S. Y. Bae, Highly conductive, stretchable and biocompatible Ag–Au core–sheath nanowire composite for wearable and implantable bioelectronics. *Nat. Nanotechnol.* **13**, 1048–1056 (2018).
48. S. Gong, L. W. Yap, B. Zhu, Q. Zhai, Y. Liu, Q. Lyu, K. Wang, M. Yang, Y. Ling, D. T. Lai, Local crack-programmed gold nanowire electronic skin tattoos for in-plane multisensor integration. *Adv. Mater.* **31**, 1903789 (2019).
49. S. H. Kim, H. Seo, J. Kang, J. Hong, D. Seong, H. J. Kim, J. Kim, J. Mun, I. Youn, J. Kim, An ultrastretchable and self-healable nanocomposite conductor enabled by autonomously percolative electrical pathways. *ACS Nano* **13**, 6531–6539 (2019).

50. L. Liu, H. Y. Li, Y. J. Fan, Y. H. Chen, S. Y. Kuang, Z. B. Li, Z. L. Wang, G. Zhu, Nanofiber-reinforced silver nanowires network as a robust, ultrathin, and conformable epidermal electrode for ambulatory monitoring of physiological signals. *Small* **15**, 1900755 (2019).
51. Y. Wang, T. Hong, L. Wang, G. Li, N. Bai, C. Li, P. Lu, M. Cai, Z. Wu, N. Lu, Epidermal electrodes with enhanced breathability and high sensing performance. *Mater. Today Phys.* **12**, 100191 (2020).

Acknowledgments: We thank S. Nagai, C. Okutani, C. Wang (The University of Tokyo, Japan), and S. Ji (Tsinghua University, China) for technical support and discussions. **Funding:** This work was supported by the Science and Technology ACCEL (Grant JPMJMI17F1), Japan.
Author contributions: Y.W. and T.S. conceived and designed the experiments. Y.W. carried out the experiments. Y.W., S.L., T.Y., H.W., Z.J., J.W., M.K., and T.S. analyzed the data and/or discussed the results. Y.W. and T.S. cowrote the paper. All authors commented on the manuscript. T.S. supervised the project. **Competing interests:** The authors declare that they have no competing interests. **Data and materials availability:** All data needed to evaluate the conclusions in the paper are present in the paper and/or the Supplementary Materials. Additional data related to this paper may be requested from the authors.

Submitted 12 March 2020
Accepted 26 June 2020
Published 12 August 2020
10.1126/sciadv.abb7043

Citation: Y. Wang, S. Lee, T. Yokota, H. Wang, Z. Jiang, J. Wang, M. Koizumi, T. Someya, A durable nanomesh on-skin strain gauge for natural skin motion monitoring with minimum mechanical constraints. *Sci. Adv.* **6**, eabb7043 (2020).